

Nanoscale

Accepted Manuscript



This is an *Accepted Manuscript*, which has been through the Royal Society of Chemistry peer review process and has been accepted for publication.

Accepted Manuscripts are published online shortly after acceptance, before technical editing, formatting and proof reading. Using this free service, authors can make their results available to the community, in citable form, before we publish the edited article. We will replace this *Accepted Manuscript* with the edited and formatted *Advance Article* as soon as it is available.

You can find more information about *Accepted Manuscripts* in the [Information for Authors](#).

Please note that technical editing may introduce minor changes to the text and/or graphics, which may alter content. The journal's standard [Terms & Conditions](#) and the [Ethical guidelines](#) still apply. In no event shall the Royal Society of Chemistry be held responsible for any errors or omissions in this *Accepted Manuscript* or any consequences arising from the use of any information it contains.

Nano-frost Array Technique to Prepare Nanoporous PVDF Membranes

Min Kyung Lee and Jonghwi Lee*

*Department of Chemical Engineering and Materials Science, Chung-Ang University,
Seoul, 156-756, Korea (South)*

To be submitted to **Nanoscale**

*To whom correspondence should be addressed. E-mail: J.L., jong@cau.ac.kr

Tel.: +82 2 8165269

Abstract: Frost, the solid deposition of water vapor from humid air, forms on the surface of a solid substrate when its temperature drops below the freezing point of water. In this study, we demonstrated how this natural phenomenon can be applied to develop novel nanoporous materials. The solvent annealing of polyvinylidene fluoride (PVDF) infiltrated in nanopores induced template-directed dewetting thus preparing nanoembossing films. Then, water nanodroplets formed on the cold polymer nanopatterned surfaces following the embossing patterns, similar to dew formation on the ground. Subsequently, the nanodroplets were frozen and then removed by freeze-drying. This nano-frost array technique produced nanoporous PVDF membranes with an average thickness of 250 (± 48) nm. It was revealed that the nanopatterned surface formed by solvent annealing played an important role in achieving a nano-frost array with an adjustable size. Additionally, the freezing process led to significant changes of the PVDF crystallinity and polymorphism. Our results prove that the nano-frost array technique can be broadly used to design ordered nanoporous structures and provide new prospects in nanomaterial fields.

Keywords: nanoporous membrane, PVDF (polyvinylidene fluoride), solvent annealing, template-directed dewetting, nano-frost array

Introduction

Frost formation is considered to be a major problem which affects a variety of industries including power generation, transportation, construction, and agriculture. Accordingly, to date, research efforts have focused on developing so-called “icephobic” surfaces that resist ice formation.¹⁻⁵ However, the concept we are introducing here is different than previous research. In this work, we demonstrated frost formation and its organization on a hydrophobic polymer layer, and suggest that this array technique can be an effective way to fabricate novel ordered nanoporous membranes.

Highly ordered polymeric films have attracted significant interest due to their potential applications in the fields of photonic crystals, catalyst substrates, templates, filtration membranes, microlens arrays, superhydrophobic surfaces, and cell culture devices.⁶⁻⁹ Although various techniques have been developed to fabricate porous films with ordered structures including lithography and templating, these methods have drawbacks including being complicated, expensive, and the inability to dynamically regulate the pore size.^{10,11} Because of the needs for simpler, cheaper, and faster processes, self-assembly and self-organization processes have attracted considerable attention over the past few decades.^{12,13}

Recently, a facile, dynamic, and economic approach to fabricate various polymeric microporous films called the breath figure (BF) method has attracted significant attention.^{14,15} BF is the fog that forms when moist air comes into contact with a cold surface. Briefly, in the presence of moisture, water is condensed on a cold surface via a nucleation and growth process. As the polymer solution continues to concentrate, the water droplets, separated by a layer of polymer, self-organize into a well-ordered pattern. Finally, a polymer film containing micropores is obtained after the removal of entrapped water droplets. Although many researchers have

developed BF-based techniques capable of fabricating polymeric films with unique morphologies,^{16,17} the exact mechanism of this process is still under investigation. Most of the techniques are not suitable for fabricating permeable films due to poor pore connectivity and many defects.¹⁸ In addition, nanoscale organization through the BF technique has, to date, seldom been reported. It has not been examined what will happen if the BF process on nanopatterned surfaces have not been investigated and moreover, previous studies concerning BF have not considered frost formation.

This paper proposes an innovative approach using a ‘nano-frost array’ technique with the support of a nanopatterned surface for the preparation of highly permeable nanoporous structures in polymeric films using the BF technique. This approach involves the following processes (**Scheme 1**): 1) polymer infiltration through the nanopores of a template, 2) exposure to a co-solvent vapor (DMAc/water), leading to the template-directed dewetting, 3) condensation of water vapor onto the cold polymer surface, forming water nanodroplets, 4) nano-frost formation at a temperature below the freezing point of water, and 5) complete removal of the frost crystals, producing nanoporous polymer membranes. We demonstrated this technique using PVDF (polyvinylidene fluoride)^{19,20} as a model semicrystalline polymer in order to examine the possibility to regulate the crystallinity and polymorphism of PVDF by using the related processing parameters. Additionally, we examined whether annealing and subsequent freezing processes could control the droplet formation and growth as well as further improve the morphological and molecular regularity of PVDF nanomembranes. We believe that this simple approach has great potential to enable various designs of polymeric membranes and functional porous materials that are not feasible using conventional methods.

Experimental

Preparation of PVDF Nanoporous Membranes

Alumina templates (AAO) with a pore size of 200 nm were purchased from Synkera Technologies (Longmont, CO). The membranes are freestanding disks with a diameter of 13 mm and a thickness of 60 μm . Each template was ultrasonically cleaned in acetone for 15 min, followed by 5 min of ultrasonic cleaning in deionized water.

Poly(vinylidene fluoride) (PVDF, average $M_w = 534\text{K g/mol}$, Sigma Aldrich) was infiltrated inside the alumina template by solution wetting. A solution containing 10 wt% PVDF in N,N-dimethylacetamide (DMAc, Sigma Aldrich) was prepared. The concentration used was determined by considering the range of concentrations reported in our previous report in which we produced high aspect ratio polymer nanorods.²¹ For solution wetting, the alumina template was placed on top of a drop of the PVDF solution and then rapidly placed on a filter paper to remove the residual solution outside the nanopores. The alumina template was subsequently dried at 60 °C under vacuum for 24 h. This first step of solution wetting is the same as that used in previous templating methods²¹, whereas the subsequent solvent-annealing step yielded completely new results allowing control of the nanostructures. For the solvent annealing process, the alumina template filled with PVDF was exposed to saturated DMAc/water vapor for different periods of times in a homemade glovebox chamber at room temperature (**Fig. S1**). The glovebox chamber had constantly circulating humid air. The relative humidity (R.H.) in the chamber was controlled by adjusting the water temperature and monitored. Once the desired R.H. condition was reached (R.H. of 90%), it was maintained constant throughout the whole process. Briefly, the sample was placed in an upside-down Teflon container containing saturated DMAc vapor as shown in **Fig. S1**. To maintain the saturated DMAc vapor, the chamber was covered by a larger Teflon container. A glass flask filled with water was placed into the large Teflon container. A

small spout in the Teflon container allowed water vapor to flow through the internal container. The sample was annealed for 20 hrs and then, the DMAc vapor was removed, allowing the DMAc in the swollen PVDF to evaporate under the given RH conditions. Within 30 sec, the sample was placed on top of a cooper plate (thickness: 0.5 mm) contacting a liquid nitrogen bath on the same way that we used in our previous study²¹. After the contact, cooling started from the bottom and spread to the top of the sample. In this step, the sample was allowed to cool rapidly for 3 min to induce freezing of the water nanodroplets and residual DMAc along the vertical direction, and recrystallize the polymer. Finally, the frozen sample was freeze-dried using an FD-1000 freeze dryer (EYELA, Tokyo, Japan, trap chilling temperature -45°C, 5.6 Pa) for 24 hrs.

Filtration Assay

The membrane with lateral dimensions of 5 mm x 5 mm was mounted in a filter module. Polystyrene microspheres (2 μm , monodisperse, Fluka) were dispersed in water with a concentration of 2 mg/mL. A syringe was used to induce the permeation of the dispersion. The filtrates were collected and analyzed.

Characterization

The nanoporous PVDF membranes were analyzed using a field emission scanning electron microscope (FESEM, SIGMA, Carl Zeiss). Images were obtained using an accelerating voltage of 2 kV and a working distance of 11 mm. Platinum layers were deposited on the samples by ion sputtering (E-1030, Hitachi, Japan). The average pore size and porosity were measured by using Scion Image software (Alpha 4.0.3.2, NIH, MD, USA). Three images (1.5 x 1 μm) of each sample were analyzed.

Using a NaOH solution (5 wt%), the nanoporous PVDF membrane was detached from the alumina template and transferred to copper grids for transmission electron microscopy (TEM)

observation. A JEOL-2000 TEM (JEOL, Peabody, MA) operating at an accelerating voltage of 200 kV and equipped with a double tilt holder was used for imaging and electron diffraction. A CCD camera (GATAN, DUAL VIEW) was used to record the images. The camera length was calibrated using a similar TEM grid coated with 10 nm of aluminum.

X-ray diffraction (XRD) measurements were obtained using a D/max (Rigaku, Japan) by the usual θ - 2θ method with a voltage of 40 kV and a Cu K α source ($\lambda=1.541 \text{ \AA}$). Grazing incidence X-ray diffraction (GIXD) measurements were performed using a four-circle diffractometer (SMARTLAB, Rigaku) with a rotating Cu anode X-ray generator. The incidence angle was fixed at 0.3° so that the X-ray beam could penetrate the entire thickness of the nanoporous membranes ($\sim 100 \text{ nm}$).

Results and Discussion

The method used for infiltrating PVDF into the nanopores of the alumina template is based on the wetting behavior of the PVDF solution over the nanopore walls. SEM images of the alumina template and the PVDF-filled nanotemplate are shown in **Fig. 1**, in accordance with our previous report.²¹ It is well known that the wettability of a solid surface is generally controlled by both its surface energy and geometrical architecture.²² Accordingly, the PVDF/DMAc solution has a low surface energy that spontaneously tends to wet the pore wall of the high surface energy alumina template.²¹ In addition, considering the pore structure and the contact angle of DMAc on the alumina surface²³, it is believed that the solution containing PVDF in DMAc readily wets the alumina surface. For the convenience of discussion, the physical properties of the solvents are summarized in **Table S1**.^{23,24}

After vacuum drying, the alumina template filled with PVDF was solvent-annealed under DMAc/water vapor for 20 hrs. Under DMAc/water vapor, the PVDF phase becomes swollen by DMAc, which is a good solvent for PVDF, while the water molecules prefer alumina surfaces. As shown **Fig. 2A-1**, after solvent annealing for a certain time, the PVDF membrane with a nanoembossing pattern could be prepared on the top surface of the nanoporous template. According to theoretical studies, the dewetting process is driven by surface and strain minimization, which can be explained by the classical nucleation and growth theory.²⁵ As DMAc molecules are absorbed, PVDF achieves enough mobility for dewetting. Water wets the alumina surface due to its good wettability on alumina²² and the repulsion between PVDF and water due to the hydrophobicity of PVDF generates a net flux of PVDF molecules out of the pores. Thus, PVDF molecules move to the top surface of the template along the walls and spread on the top surface, resulting in a continuous film being connected with nanoembossing units. Due to the flux out of the pores, PVDF molecules exit from inside the pores, similar to a volcanic eruption. As a result, the ‘crests-and-troughs’ pattern morphology forms reflecting the nanostructures of the nanoporous alumina templates (**Fig. 2A-2**). The substrate pattern strongly influences the dewetting pathways as well as the organization and size of the nanostructures (**Fig. 2A-1**).²⁶

Finally, the nanopores are formed over the entire membrane by subsequent freezing (**Fig. 2B-1**). Such pore formation can be explained by the BF concept. In this concept, the fog created by exhaling on a cold PVDF surface is obtained under a humid environment (**Fig. 2B-2**). Briefly, consecutive evaporation of DMAc leads to a decrease of the air/liquid interfacial temperature. This evaporative cooling induces the condensation of water droplets on the surface of the PVDF nanofilm. With further evaporation of DMAc, the growth of water droplets may be confined by PVDF nanoembossing units around the droplets in the ‘trough’. This confinement effect enables

nano-frost formation, differing from most BF processes which usually form micro-sized droplets. Therefore, it should be noted that the nanoembossing pattern obtained by solvent annealing is a crucial parameter that determines the uniform size of water droplets and develops the 2D arrays since it plays an important role in the stabilization of water droplets. It should be also noted that the underlying template is an important parameter in the control of final structure.

The growth of water droplets on the nanopatterned surface is quite different from the general growth mechanism, in which diffusion-limited growth and coagulative growth occur simultaneously, leading to a relatively broad size distribution.²⁷ In light of the results, it is believed that water droplets are trapped between nanoembossing units and stabilized by the trough-like geometry (**Fig. 2B-2**). Then, droplets may grow as isolated forms, resulting in the narrow size distribution (diffusion-limited growth). Afterwards, the residual DMAc and water droplets are completely frozen and then removed, leaving behind an imprint of the ice crystals (frost) with an average size of 150 nm in the PVDF matrix (**Fig. 2B-2**). Furthermore, after being detached from the templates, the PVDF nanoporous membranes with an average thickness of 250 (± 48) nm possess a highly permeable structure, demonstrating that it has through-thickness pores. Although the edge of dried nanomembrane was slightly shrunken, the tilted view of SEM image shows that the thickness of the detached nanomembrane is about 200 nm (**Fig. S2**). For the complete cycle of nanoporous membrane preparation, the dissolution of AAO is not necessary. TEM images of a representative PVDF membrane with through-thickness nanopores are shown in **Fig. 3**. Moreover, the nanomembrane with typical lateral dimensions of 5 mm x 5 mm could float on a water surface and were easily picked up using a pair of tweezers (**Fig. S3**). Additionally, we also demonstrated the separation performance of prepared nanomembranes (**Fig.**

S4).²⁸ Therefore, this method would allow the well-controlled fabrication of freestanding nanomembranes in order to improve their applicability such as separation.

Furthermore, we note that the pore morphology depends on the annealing time. A humid exposure leads to a transfer of water from the vapor phase into the swollen PVDF matrix. The extent of water transfer can be controlled by adjusting the exposure time. Moreover, the morphology of the semicrystalline polymer membrane is caused by two types of phase separation processes: liquid-liquid demixing and solid-liquid demixing (polymer crystallization) or their competition. The sequence of events in the phase separation process depends upon kinetic parameters. In this experiment, following the intake of water from the humid air, PVDF had sufficient time to crystallize. There is less time for in-diffusion of water, hence a crystallization-controlled morphology is obtained. As shown in **Fig. 4A**, **Fig. 4B**, and **Fig. 5**, a short annealing time (1-5 h) led to the preferential formation of pores with sizes of 4-50 nm, while the pore size ranged from 100 to 120 nm after annealing for 10 h (**Fig. 4C** and **Fig. 5**). A longer time (20 hrs, **Fig. 2B-1**, **Fig. 4D**, and **Fig. 5**) led to membranes with well-developed pores with sizes of 150-200 nm. In addition, the annealing time affects the 2D porosity, indicating the amounts of water and DMAc in the PVDF matrix (**Fig. 5**). After 7 days, the average pore size was 500 nm. Under this condition, the absorbed water was enough to cause phase separation in the entire membrane. This phenomenon can be explained as follows. The film is in the metastable region in the phase diagram of DMAc/water/PVDF system²⁹, which is rather close to the spinodal line. As the samples are annealed for longer times, spinodal decomposition and subsequent crystallization can occur. This led to the structure consists of a lace-like structure of loosely connected spheres (**Fig. 4E** and **F**). Therefore, it is considered that the exposure time dominated the phase separation, due to the fraction of water absorbed from the humid air. This

subsequently affects the solvent crystal size with the consequent effects on the pore size. (**Fig. 4** and **Fig. 5**).

To understand what occurs during co-solvent annealing, we take into account the physical properties and miscibility between water droplets (atmospheric vapor) and DMAc (swollen polymer layer). It is well-known that the shape of the droplet is mainly determined by the interfacial tension between the droplet and polymer solution instead of the air-water interface. The droplet formation on the swollen polymer layer is schematically shown in **Fig. 6**. The spreading coefficient, S , which is the Gibbs free energy change in spreading water droplets over a unit area of the polymer surface, is defined as³⁰

$$S = \gamma_{sg} - (\gamma_{wg} + \gamma_{ws}) \quad (1)$$

where γ_{sg} is the surface tension of the swollen polymer layer, γ_{wg} is the surface tension of a water droplet, and γ_{ws} is the interfacial tension between the swollen polymer and a water droplet ($\gamma_{DMAc} = 24$ mN/m; $\gamma_{PVDF} = 28.6$ mN/m; $\gamma_{water} = 72.8$ mN/m)^{31,32}. $S > 0$ corresponds to complete wetting and $S < 0$ indicates partial wetting. In this system, the values of γ_{ws} are speculated to be small or even zero because water is miscible with DMAc. Therefore, the S value is expected to be positive. Once the water droplets appear on the surface of the PVDF/DMAc layer, they will tend to spread at the air-solution interface. Therefore, the water droplets fused into bigger droplets over time and penetrated into the DMAc phase. The droplets are absorbed into the PVDF layer and eventually mix with DMAc, leading to partial collapse of the PVDF structure. Concurrently, PVDF precipitation may take place during annealing since water is a non-solvent for PVDF. Therefore, an excessive annealing time tends to increase the degree of PVDF supersaturation, leading to a disordered structure and low porosity (**Fig. 4F** and **Fig. 5**). The timely exposure to a co-solvent is a key factor in the maintenance of a highly ordered structure.

As shown in **Fig. 7**, the lack of an X-ray diffraction peak for the non-annealed films indicates an amorphous-like structure. When exposed to water/DMAc for 1 h, there were no significant differences in the diffraction patterns. In contrast, after annealing for 5 hrs, two peaks appeared at 2θ values of 18.5° and 20.1° corresponding to the (020) and (110) reflections of the γ phase crystal, respectively, which increased in intensity when the annealing time was extended to 20 hrs. However, after 7 days of exposure, both peaks at 18.5° and 20.8° decreased, indicating a discontinued increase in accordance with the SEM and DSC results (**Fig. 4** and **Fig. S5**). As mentioned above, water and DMAc can be mixed together with prolonged annealing, where the mobility of a polymer chain progressively increases with increasing annealing time, leading to poor ordering. The two major factors which affect the PVDF crystallization, the amount of the solvent and the composition, changed as a function of the annealing time. Therefore, it is reasonable to speculate that there is an optimum solvent annealing time and an appropriate choice of solvent to maximize the order of the structure.

To investigate whether the freezing process (frost formation) has an effect on the crystal structure of nanoporous membranes, grazing incidence X-ray diffraction experiments were conducted. As shown in **Fig. 8A**, a broad α -phase peak at $2\theta = 17.6^\circ$ corresponding to the (100) reflection is mainly present in the PVDF membrane before solvent annealing. However, in the solvent-annealed PVDF film (**Fig. 8B**), which was prepared through solvent annealing and evaporation instead of freezing, small γ -phase peaks at 18.5° and 20.8° are present, which indicates the existence of a small percentage of a ferroelectric γ -phase along with the α -phase. As shown in **Fig. 8C**, the peaks at 18.5° and 20.8° become progressively sharper and better defined as freezing is applied. This indicates that the combination of annealing and subsequent freezing provides the possibility to increase the crystallinity, as well as polymorphic

controllability. In light of these results, the PVDF chains may rearrange themselves for the formation of the γ phase in the early stage of crystal nucleation during solvent annealing. The subsequent freezing process induces the crystallization of ice (T_m : 0°C) and DMAc (T_m : -20°C), and then polymer chains would be excluded from the solvent crystals with the development of a concentration gradient in the unfrozen part of the system in front of the growing crystals. Finally, PVDF chains would be aligned by the transfer of heat across the moving freezing front and subsequent solvent crystallization, thus allowing the possible formation of highly-ordered crystalline phases (**Fig. 8C**). Although various ways to obtain ferroelectric γ -phase of PVDF have been attempted, a fabrication method which can control the pore morphology and crystal structure has rarely been reported³³⁻³⁶. Moreover, this fabrication method which can form highly-ordered crystalline phase would be broadly useful in controlling semicrystalline polymers, because the material's crystallinity affects the resulting mechanical properties (**Fig. S3**).

Common AAO nanotemplating methods are not efficient since the detachment of templates is the most difficult step in the entire process, resulting in low production yields. In this step of AAO dissolution, nanostructures are often broken or damaged. However, our method produced nanomaterials with an unexpected nanomembrane morphology, not nanowires or nanoparticles which are typically obtained from nano-templating methods of AAO. Therefore, our nano-frost array technique does not require a harsh detachment step, which is advantageous to prepare defect-free nanostructures and further provide repeatedly usable templates. The amount of infiltrated polymers as well as the spacing and size of AAO pores conveniently determined the thickness and pore size of the nanoporous membranes.

Conclusion

BF arrays can introduce micropores into various polymer systems but there have been no attempts to generate and organize nanopores using the BF mechanism. This study demonstrated that a simple but unprecedented process to develop nano-frost array can be used to prepare nanoporous membranes. One of the highlights of this technique is the capability to arrange nano-frost crystals on a polymer surface. It was found that the nanopatterned surface of the polymer matrix is important in confining and organizing nano-frost crystals. Through this technique, PVDF nanomembranes with through-thickness pores could be obtained. Additionally, the regularity of the nanomembranes could be explained based on the physical properties of the solvent used including its surface tension and solubility. Furthermore, the freezing process for frost formation can provide enhanced crystallinity and polymorphic controllability. It should be also noted that the choice of suitable solvent for the polymer is paramount in this approach. Once chosen, the rest of procedure can follow the method described in this work. Therefore, we believe that this procedure can be applied to various polymer materials. We believe that this novel strategy is valuable when designing and fabricating ordered nanomembranes and it offers a facile way to control the morphological features of nanostructures.

Acknowledgements. This work was supported by National Research Foundation grants funded by the Korean Ministry of Science, ICT, and Future Planning (NRF-2012R1A2A2A01014107 and NRF-2013R1A1A2021573).

References

- [1] S. Jung, M. Dorrestijn, D. Raps, A. Das, C. M. Megaridis and D. Poulidakos, *Langmuir*, 2011, **27**, 3059-3066.
- [2] P. Tourkine, M. Le Merrer and D. Quere, *Langmuir*, 2009, **25**, 7214-7216.
- [3] A. J. Meuler, J. D. Smith, K. K. Varanasi, J. M. Mabry, G. H. Mckinley and R. E. Cohen, *ACS Appl. Mater. Interfaces*, 2010, **2**, 3100-3110.
- [4] K. K. Varanasi, T. Deng, J. D. Smith, M. Hsu and N. Bhate, *Appl. Phys. Lett.*, 2010, **97**, 234102.
- [5] S. Jung, M. K. Tiwari, N. V. Doan and D. Poulidakos, *Nat. Commun.* 2012, **3**, 615.
- [6] L. S. Wan, J. W. Li, B. B. Ke and Z. K. Xu, *J. Am. Chem. Soc.*, 2012, **134**, 95-98.
- [7] A. Boker, Y. Lin, K. Chiapperini, R. Horowitz, M. Thompson, V. Carreon, T. Xu, C. Abetz, H. Skaff, A. D. Dinsmore, T. Emrick and T. P. Russell, *Nat. Mater.* 2004, **3**, 302-306.
- [8] D. J. Harris and J. A. Lewis, *Langmuir*, 2008, **24**, 3681-3685.
- [9] J.-H. Lee, H.W. Ro, R. Huang, P. Lemaillet, T.A. Germer, C.L. Soles and C.M. Stafford, *Nano Lett.*, 2012, **12**, 5995-5999.
- [10] M. L. K. Hoa, M. H. Lu and Y. Zhang, *Adv. Colloid Interface Sci.*, 2006, **121**, 9-23.
- [11] U. H. F. Bunz, *Adv. Mater.*, 2006, **18**, 973-989.
- [12] M. Templin, A. Frank, C. A. Du, A. Leist, A. Zhang, R. Ulrich, V. Schalder and U. Wiesner, *Science*, 1997, **278**, 1795-1798.
- [13] T. Thurn-Albrecht, R. Steiner, J. DeRouchey, C. M. Stafford, E. Huang, M. Bal, M. Tuominen, C. J. Hawker and T. P. Russell, *Adv. Mater.*, 2000, **12**, 787-791.
- [14] G. Widawski, M. Rawiso, B. Francois, *Nature*, 1994, **369**, 387-389.
- [15] H. Bai, C. Du, A. Zhang and L. Lei, *Angew. Chem. Int. Ed.*, 2013, **52**, 2-18.
- [16] B. de Boer, U. Stalmach, H. Nijland and G. Hadziioannou, *Adv. Mater.*, 2000, **12**, 1581-

1583.

[17] H. Battendo, R. J. Cobley and S. P. Wilks, *Soft Matter*, 2011, **7**, 10864-10873.

[18] H. Ma, J. Cui, A. Song and J. Hao, *Chem. Commun.*, 2011, **47**, 1154-1156.

[19] A. J. Lovinger, *Macromolecules*, 1981, **14**, 322-325.

[20] M. Kobayashi, K. Tashiro and H. Tadokoro, *Macromolecules*, 1975, **8**, 158-171.

[21] M. K. Lee and J. Lee, *Cryst. Growth Des.*, 2013, **13**, 671-678.

[22] P. D. Mingfu Zhang, J. T. Chen and T. P. Russell, *Nano Lett.*, 2006, **6**, 1075-1079.

[23] D. J. Trevoy and H. Jr. Johnson, *J. Phys. Chem.*, 1958, **62**, 833-837.

[24] G. A. Miner and D. M. Stoakley, A. K. St Clari, P. A. Gierow and K. Bates, Technical report, NASA, 1997.

[25] D. T. Danielson, D. K. Sparacin, J. Michel and L. C. Kimerling, *J. Appl. Phys.*, 2006, **100**, 083507.

[26] R. Mukherjee, D. Bandyopadhyay and A. Sharma, *Soft Matter*, 2008, **4**, 2086-2097.

[27] A. E. Saunders, J. L. Dickson, P. S. Shah, M. Y. Lee, K. T. Lim, K. P. Johnston and B. A. Korgel, *Phys. Rev.*, 2006, **E73**, 031608.

[28] L. -S. Wan, J. -W. Li, B. -B. Ke, and Z. -K. Xu. *J. Am. Chem. Soc.*, 2012, **134**, 95-98.

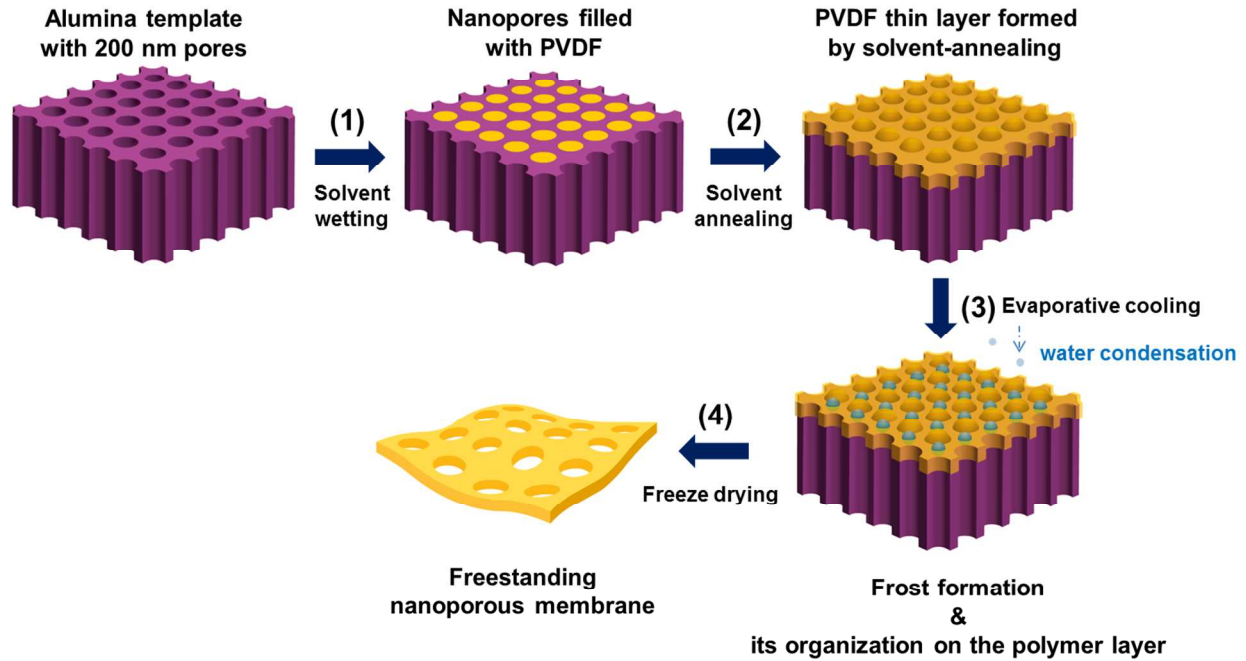
[29] P. Yuelian, F. Hongwei, G. Ju, W. Shaobin, C. Ping, and J. Qi, *Appl. Surf. Sci.* 2012, **263**, 737-744.

[30] M. Morra, C. D. Volpe and S. Siboni, *Polymer Interfaces and Emulsions*, New York, 1999, p559.

[31] D. M. Koenhen, C. A. Smolders, *J. Appl. Polym. Sci.*, 1975, **19**, 1163-1179.

[32] A. C. M. Franken, J. A. M. Nolten, M. H. V. Mulder, D. Bargeman, and C. A. Smolders, *J. Membrane Sci.*, 1987, **33**, 315-328.

- [33] Z. Hu, G. Baralia, V. Bayot, J. F. Gohy and A. M. Jonas, *Nano Lett.*, 2005, **5**, 1738-1743.
- [34] A. J. Lovinger, *Science*, 1983, **220**, 1115-1121.
- [35] T. Furukawa, *Adv. Collloid Interface Sci.* 1997, **71**, 183-208.
- [36] R. Hasegawa, Y. Takahashi, Y. Chatani and H. Tadokoro, *Polym. J.* 1972, **3**, 600-610.



Scheme 1. Schematic representation of the formation of ordered nanoporous membranes by the nano-frost array technique.

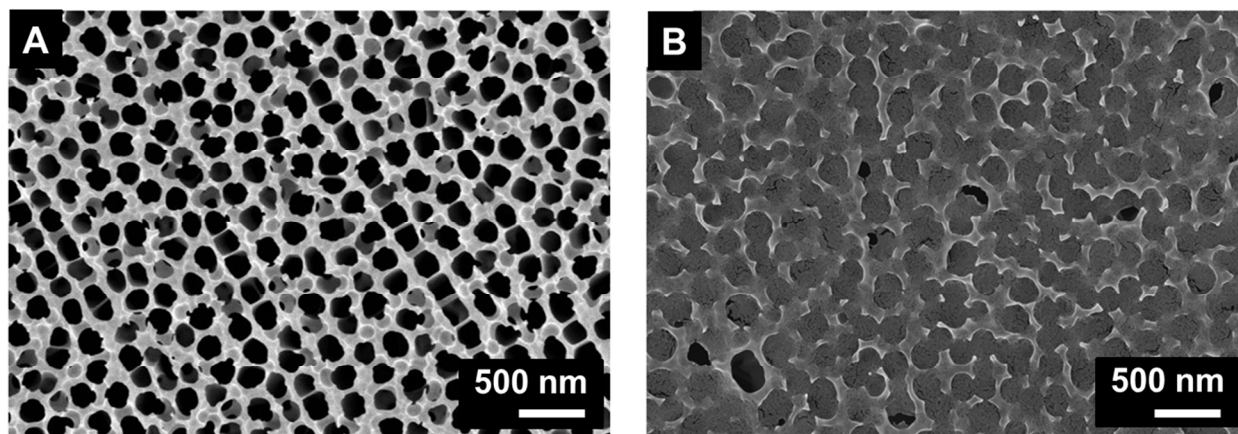


Figure 1. SEM images of the surfaces of (A) a bare alumina template with 200 nm diameter pores and (B) PVDF infiltrated into an alumina template.

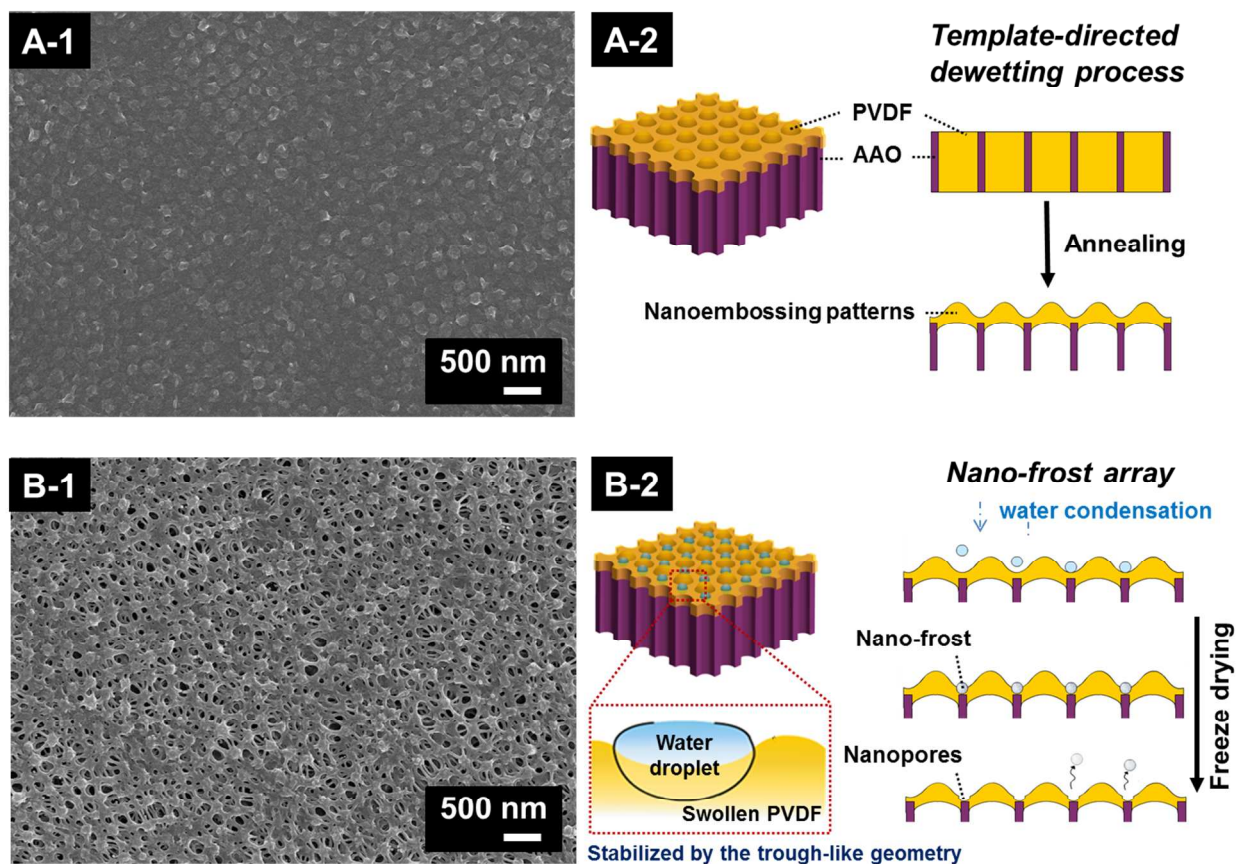


Figure 2. SEM images of (A-1) a PVDF nanoembossing film formed by template-directed dewetting under co-solvent vapor, (B-1) a nanoporous PVDF layer formed by the nano-frost array method under a humid environment, and illustrations of the proposed (A-2) dewetting and (B-2) nanopore formation processes.

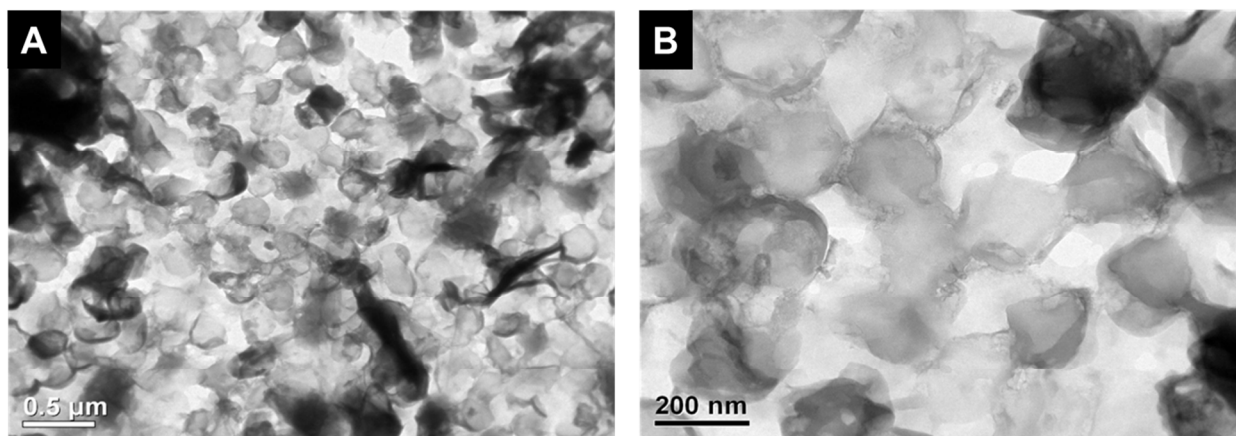


Figure 3. TEM images of (A) PVDF nanomembranes prepared using the nano-frost array method and (B) a magnified image of (A).

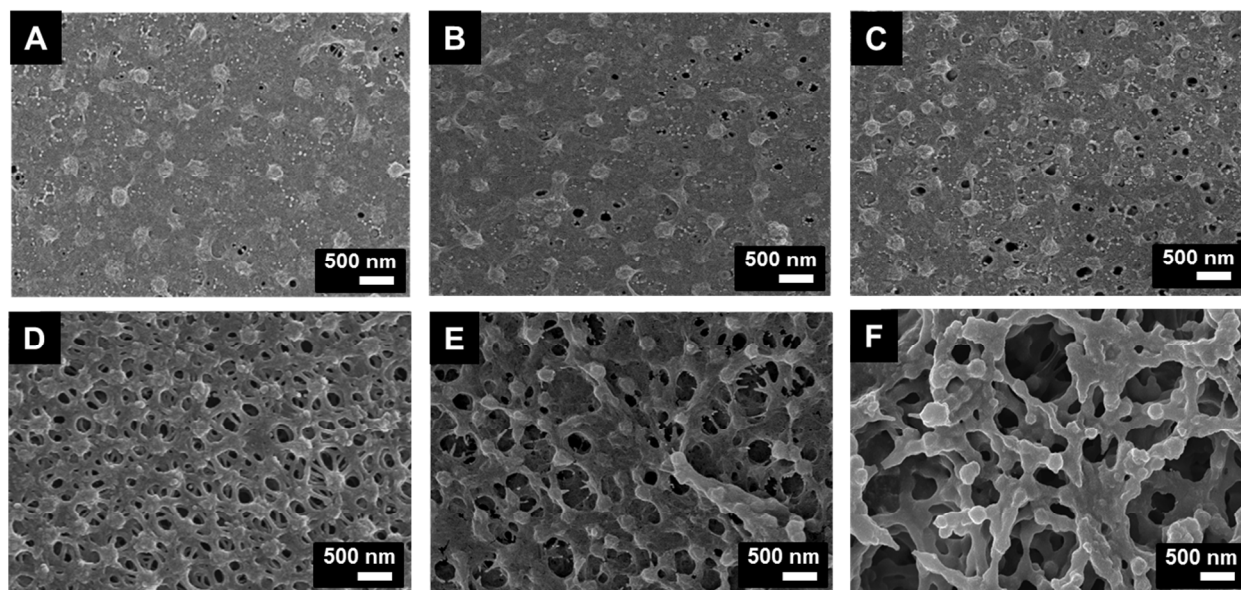


Figure 4. SEM images of porous PVDF membranes after solvent annealing for different times:

(A) 1 h, (B) 5 h, (C) 10 h, (D) 20 h, (E) 40 h, and (F) 7 days.

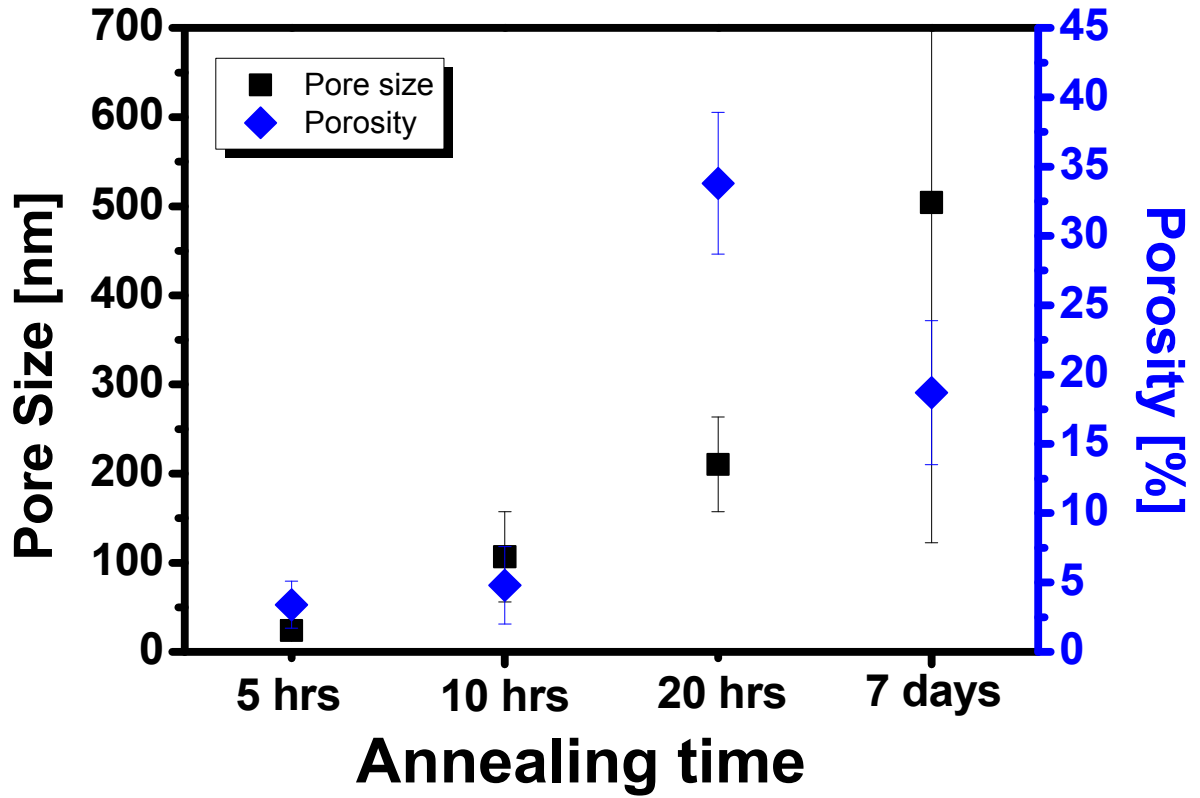


Figure 5. Average pore size and porosity of the PVDF nanomembranes as a function of the annealing time.

Condensation of vapor (water)

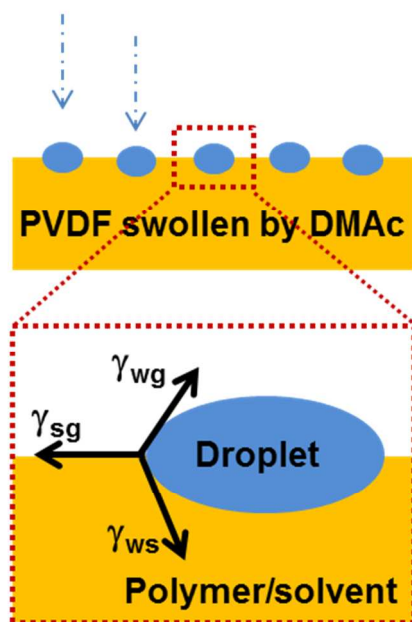


Figure 6. Schematic representation of the nanodroplet formation on the swollen PVDF layer (polymer/solvent).

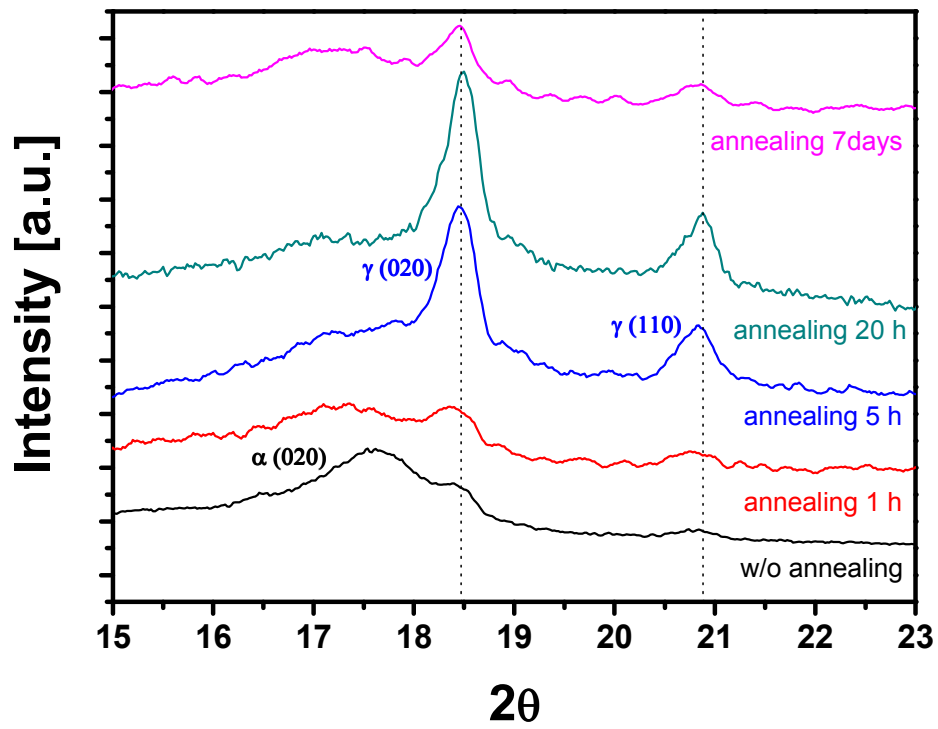


Figure 7. Grazing incidence X-ray diffraction patterns of PVDF nanomembranes prepared under different annealing times.

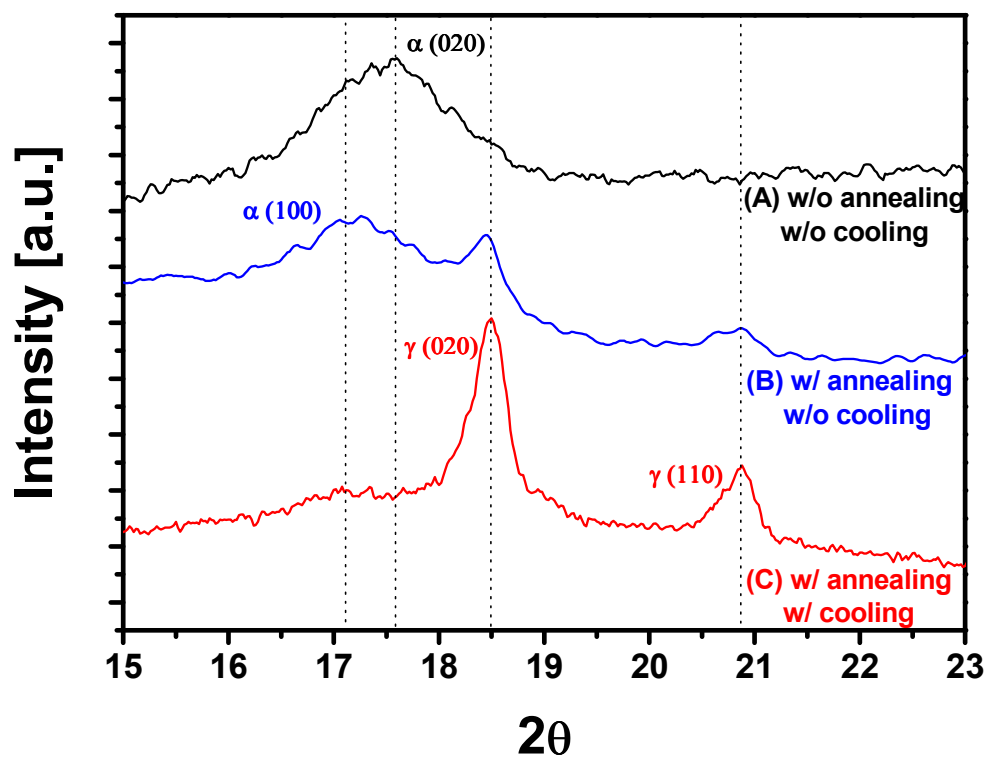
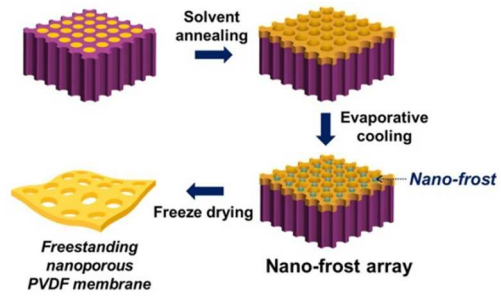


Figure 8. Grazing incidence X-ray diffraction patterns of PVDF nanomembranes prepared under different conditions.

Graphic Abstract



We demonstrate a simple but novel approach to fabricate nanoporous polymer membranes by nano-frost array technique.